

# Vibrational States of Glassy and Crystalline Orthoterphenyl

A. Tölle<sup>1</sup>, H. Zimmermann<sup>2</sup>, F. Fujara<sup>3</sup>, W. Petry<sup>4</sup>, W. Schmidt<sup>5</sup>, H. Schober<sup>5</sup>, and J. Wuttke<sup>4</sup>

<sup>1</sup> Fachbereich Physik, Universität Dortmund, 44221 Dortmund, Germany

<sup>2</sup> Max-Planck-Institut für medizinische Forschung, 69120 Heidelberg, Germany

<sup>3</sup> Institut für Festkörperphysik, Technische Universität Darmstadt, 64289 Darmstadt, Germany

<sup>4</sup> Physik-Department E13, Technische Universität München, 85747 Garching, Germany

<sup>5</sup> Institut Laue-Langevin, 38042 Grenoble, France

November 17, 2018

**Abstract.** Low-frequency vibrations of glassy and crystalline orthoterphenyl are studied by means of neutron scattering. Phonon dispersions are measured along the main axes of a single crystal, and the corresponding longitudinal and transversal sound velocities are obtained. For glassy and polycrystalline samples, a density of vibrational states is determined and cross-checked against other dynamic observables. In the crystal, low-lying zone-boundary modes lead to an excess over the Debye density of states. In the glass, the boson peak is located at even lower frequencies. With increasing temperature, both glass and crystal show anharmonicity.

**PACS.** 61.43.Fs Glasses – 63.50.+x Vibrational states in disordered systems – 63.20.-e Phonons in crystal lattice – 61.12-q Neutron diffraction and scattering

## 1 Introduction

Orthoterphenyl (OTP) has been studied for more than forty years as prototype of a non-associative, non-polar molecular glass former [1]. Early studies concentrated on viscosity [1, 2, 3, 4, 5, 6] and  $\alpha$ -relaxation [7, 8, 9, 10, 11, 12, 13, 14] as direct manifestations of the frequency-dependent glass transition, or on slow  $\beta$  relaxation [15, 16, 17].

In the past decade, a new frame has been set by mode-coupling theory [18, 19, 20] which describes the onset of structural relaxation on microscopic time scales. Consequently, the fast dynamics of OTP has been studied by incoherent [21, 22, 23, 24, 25] and coherent [26, 27, 28] inelastic neutron scattering as well as by depolarised light scattering [29, 30, 31] and is found to be in good accord with asymptotic results of theory.

Closed formulations of mode-coupling theory exist only for very simple systems consisting of spherical particles [32] or mixtures thereof [33], and the generalisation to dipolar molecules requires already intimidating formal efforts [34, 35]. Intramolecular vibrations have not yet been explicitly considered, and therefore the fit of mode-coupling asymptotes to complex systems like OTP remains heuristic. Worse: theoretical studies of a hard-spheres system [36, 37] have shown that the full asymptotic behaviour is only reached when the relaxational time scale is separated by several orders of magnitude from the microscopic dynamics, whereas experimental studies are restricted to at best three decades in time or frequency. On this background the present communication shall supplement our

neutron scattering studies of relaxational dynamics in OTP [21, 22, 23, 24, 25, 26, 27, 28] by an explicit investigation of vibrational states.

As other glasses, OTP possesses more low-frequency modes than expected from the Debye model. This excess, for obscure reasons named “boson-peak”, is usually taken as a characteristic feature of disordered systems. To substantiate this interpretation, glasses and crystals must be compared systematically, which so far has been done for very few systems [38, 39, 40, 41, 42, 43, 44, 45, 46, 47, 48].

OTP crystallises easily into a polycrystalline powder. Some effort is needed to prevent it from crystallisation when cooling below the melting point  $T_m=329$  K. It forms a stable glassy structure when it is supercooled below the caloric glass transition temperature  $T_g=243$  K. One particular advantage is that large single crystal specimens of several  $\text{cm}^3$  can be grown. So we are able to compare scattering from a single crystal, from powder-like polycrystal, and from the glass.

The paper is organised as follows: The analysis of single crystal dispersion relations in Sec. 2 enables us to fix the frequency range of acoustic modes in the ordered state. The vibrational density of states and the derived thermodynamic quantities of the glass and the polycrystal are compared with each other in Sec. 3. The temperature effect on the frequency distributions in the crystal and the glass is presented in Sec. 4.

## 2 Single Crystal: Phonon Dispersions

### 2.1 Structural Information

The OTP molecule (1,2-diphenyl-benzene:  $C_{18}H_{14}$ ) consists of a central benzene ring and two lateral phenyl rings in ortho position.

The crystal structure belongs to the orthorhombic space group  $P2_12_12_1$  with four molecules per unit cell and lattice parameters  $a = 18.583 \text{ \AA}$ ,  $b = 6.024 \text{ \AA}$ ,  $c = 11.728 \text{ \AA}$  at room temperature [49,50]. A sketch of the structure is given in Fig. 1 of Ref. [49].

For steric reasons, the lateral phenyl rings are necessarily rotated out of plane. In addition, the overcrowding in the molecule leads to significant bond-angle and out-of-plane distortions of the phenyl-phenyl bonds. Such structural irregularities may explain why OTP can be undercooled far easier than *m*- or *p*-terphenyl [1].

In the crystal, the angles for the out-of-plane rotation of the lateral phenyl rings are  $\phi_1 \simeq 43^\circ$  and  $\phi_2 \simeq 62^\circ$  [49,50]. For isolated molecules, an old electron diffraction study had suggested  $\phi_1 = \phi_2 = 90^\circ$ , but newer experiments and calculations agree that in the gas or liquid phase  $40^\circ \lesssim \phi_1, \phi_2 \lesssim 65^\circ$  [51].

### 2.2 Triple-Axis Experiment

For coherent neutron scattering, perdeuterated OTP ( $C_{18}D_{14}$ ,  $> 99\%$  deuteration) was used. Single crystals of high quality and considerable size (several  $\text{cm}^3$ ) were grown out of hot methanol solution either by very slow cooling or by evaporation over several months. They grew preferentially along the shortest axis  $b$ .

The phonon dispersion measurements were carried out on a specimen of about  $1 \times 1 \times 2 \text{ cm}^3$  for temperatures between 100 and 310 K. The experiments were performed on the cold triple-axis spectrometer IN12 at the Institut Laue Langevin (ILL), mostly with constant final wave vector  $k_f = 1.55 \text{ \AA}^{-1}$ .

The lattice parameters as measured on IN12 at room temperature  $a = 18.53 \text{ \AA}$ ,  $b = 6.02 \text{ \AA}$ ,  $c = 11.73 \text{ \AA}$  are in good agreement with the literature results from neutron [49] and X-ray diffraction [50]. On cooling to 100 K,  $a$  and  $c$  change only by a few ppm, whereas  $b$  contracts by about 3%.

### 2.3 Acoustic Phonons

In Fig. 1 we present the measured phonon dispersion of crystalline OTP at 200 K along the three main symmetry directions [100], [010], and [001]. Within the available beam time not all acoustic modes could be investigated. Some optic phonons were detected as well, but not studied in detail; as an example, the lowest optic branch in [010] direction is included in Fig. 1.

Due to the crystal symmetry modes of longitudinal and transverse character are pairwise degenerated at the Brillouin zone boundary. A first interesting point is that

purely acoustic modes are confined to a rather small frequency range: crossing with optic-like branches occurs already at about 0.6 THz.

Lattice dynamics calculations [41] agree qualitatively with the measured acoustic dispersions. For instance, the crossing of the longitudinal acoustic mode in [010] direction with optic branches is predicted correctly. Quantitatively, the measured acoustic dispersions are considerably steeper than calculated. The sound velocities, determined from the initial slopes, are summarised in Table 1; they lie 20–60% above the calculated values. In all lattice directions, longitudinal sound modes are almost twice as fast as transverse modes.

The single crystal data may also be compared with sound velocities in the glass. Results from Brillouin scattering are summarised in Table 2. Taking the simple arithmetic average over the three crystal axes, the mean longitudinal and transverse sound velocities  $\langle v_{L,T} \rangle$  exceed those of the glass by about 20% and 27%, respectively.

## 3 Glass and Polycrystal: Density of Vibrational States

### 3.1 Density of States and Neutron Scattering

In the absence of crystalline order, it is no longer possible to measure selected phonon modes with well-defined polarisation and propagation vector. For polycrystalline or amorphous samples, the distribution of vibrational modes can be conveyed only in form of a spectral density of states (DOS).

In principle, the DOS can be measured in absolute units by incoherent neutron scattering. However, as soon as one goes beyond the simplest textbook example of a harmonic, monoatomic, polycrystalline solid with a simple (ideally cubic) lattice, several difficulties arise and the very concept of a DOS becomes problematic.

In a molecular solid, different atoms  $j$  participate in given vibrational modes  $r$  with different amplitudes  $e_j^r$ . Therefore, atoms in non-equivalent positions have different vibrational densities of states  $g_j(\nu)$ . In neutron scattering, these  $g_j(\nu)$  are weighted with the scattering cross sections  $\sigma_j$ . In the case of protonated OTP, we see almost only incoherent scattering from hydrogen. Worse, in the scattering law  $S(q, \nu)$  the  $g_j(\nu)$  of non-equivalent hydrogen atoms are weighted with a prefactor  $|e_j^r|^2$  and a Debye-Waller factor that depends also on  $j$ .

Only for low-frequency, long-wavelength vibrations the molecules (or some structural subunits) move as rigid bodies, the  $g_j(\nu) = g(\nu)$  become the same for all  $j$ , and the  $e_j^r$  become independent of  $r$  [24,52]. In this limit, the determination of  $g(\nu)$  from a neutron scattering law remains meaningful and feasible.

### 3.2 Experiments and Data Reduction

Vibrational spectra from glassy OTP between 160 and 245 K have been analysed previously [24]. For the present

comparison, we measured incoherent scattering from the glass at 100 K, and from the polycrystalline powder at 100, 200, and 300 K on the time-of-flight spectrometer IN6 at the ILL with an incident wavelength of 5.1 Å. If not stated otherwise, we refer in the following to the 100 K data. In these experiments, protonated OTP was used. OTP of > 99 % purity was bought from Aldrich and further purified by repeated vacuum distillation.

The raw data were converted into  $S(2\theta, \nu)$  and the container scattering subtracted. Without interpolating to constant wavenumbers  $Q$ , we calculated the DOS directly from  $S(2\theta, \nu)$ , preferentially using data from large scattering angles  $2\theta$ . Multi-phonon contributions were calculated by repeatedly convoluting  $g(\nu)$  with itself and subtracting it from  $S(2\theta, \nu)$  in an iterative procedure, as described in detail in [24].

The so-obtained DOS shows a pronounced gap above  $\nu_g \simeq 5$  THz. Comparing our results with model calculations [53], we assign all vibrations below  $\nu_g$  to the 16 degrees of freedom needed to describe the crystal structure. For 16 low-lying modes in a molecule with 32 atoms, we expect an integrated DOS

$$\int_0^{\nu_g} d\nu g(\nu) = \frac{16}{32} = 0.5. \quad (1)$$

This condition is used to readjust the absolute scale of  $g(\nu)$ . In the Appendix, we argue that the difference between measured and re-normalised  $g(\nu)$  is mainly an effect of multiple scattering.

### 3.3 Density of States in Orthoterphenyl

Fig. 2 shows the DOS of glassy and crystalline OTP at 100 K. Rather broad distributions are found for both phases. In the glass a first shoulder around 1.5 THz is followed by a second at 3.5 THz in accordance with results from Raman studies [41, 54]. As expected, the crystal DOS is more structured, in particular in the low energy region. Distinct peaks at 0.6, 0.8, 1.1 and 1.5 THz become apparent. They are due to strong contributions from zone-boundary modes, as can be seen from Fig. 1. Compared to the glass, significant density is missing in the low energy region and in the range from 1.5 to 3 THz, and reappears at higher frequencies around 3.5 THz.

In order to show the low energy modes on enhanced scale, we plot in Fig. 3  $g(\nu)/\nu^2$  which in the one-phonon approximation is proportional to  $S(Q, \nu)$  itself. In this representation, the excess of the glass over the crystal becomes evident. A well defined frequency peak appears around 0.35 THz which is downshifted with respect to the first peak of the crystal at 0.6 THz and superposed to a long tail which is similar for glass and crystal. Note that the maximum of the boson peak at 0.35 THz is located below the lowest acoustic zone-boundary phonons in the crystal.

The DOS of the polycrystalline sample is in accord with the measured dispersion of the single crystal: A small shoulder at 0.4 THz can be attributed to the transverse

acoustic zone-boundary phonons in [100] direction, and the main peak at 0.6 THz corresponds to the transverse acoustic zone-boundary phonons in the other two lattice directions. The peak at 0.8 THz reflects the longitudinal acoustic zone-boundary phonon in [001] direction and the transverse optic in [010] direction.

We performed additional coherent scattering experiments on a deuterated sample, which show that the frequency of the boson peak maximum has no dispersion for wave numbers in the range 0.8 to  $2 \text{ \AA}^{-1}$ . Its intensity is modulated in phase with the static structure factor, in accordance with observations in other glasses [44, 55].

### 3.4 Mean Square Displacement

Another dynamic observable which can be obtained from neutron scattering is the atomic mean square displacement  $\langle r^2(T) \rangle$ . Roughly speaking,  $\langle r^2(T) \rangle^{3/2}$  measures the volume to which an atom remains confined in the limit  $t \rightarrow \infty$ .

For a large class of model situations (harmonic solid, Markovian diffusion, ...) it can be obtained directly from the Gaussian  $Q$  dependence of the elastic scattering intensity

$$S(Q, \nu=0) = \exp(-Q^2 \langle r(T)^2 \rangle). \quad (2)$$

For a harmonic solid,

$$\langle r(T)^2 \rangle = \frac{\hbar^2}{6Mk_B T} \int_0^\infty d\nu \frac{g(\nu)}{\beta} \coth\left(\frac{\beta}{2}\right) \quad (3)$$

with  $\beta = \hbar\nu/k_B T$  crosses over from zero-point oscillations  $\langle r^2(0) \rangle$  to a linear regime  $\langle r^2(T) \rangle \propto T$  [56]. In any real experiment, which integrates over the elastic line with a resolution  $\Delta\nu$ , one measures actually atomic displacements within finite times  $t_\Delta \simeq 2\pi/\Delta\nu$ .

Fig. 4 shows mean square displacements of OTP, determined according to (2) from elastic back-scattering (fixed window scans on IN13, with  $t_\Delta \simeq 100 - 200$  psec) and from Fourier-deconvoluted time-of-flight spectra (taking the plateau  $S(Q, t_\Delta)$  with  $t_\Delta \simeq 5 - 10$  psec from IN6 data that were Fourier transformed and divided through the Fourier transform of the measured resolution function). For the glassy sample, a direct comparison can be made and shows good agreement between IN6 and IN13. In the polycrystalline sample, the displacement is for all temperatures smaller than in the glass.

The lines in Fig. 4 are calculated through (3) from the DOS at 100 K. For low temperatures, the  $\langle r^2(T) \rangle$  are in full accord with the values determined through (2). This comparison can be seen as a cross-check between the analysis of elastic and inelastic neutron scattering data.

Equation (3) gives not only the absolute value of  $\langle r^2(T) \rangle$ , but enables us also to read off which modes contribute most to the atomic displacement. To this end, we restrict the integration (3) to modes with  $0 < \nu < \nu'$ . The inset in Fig. 4 shows the relative value  $\langle r^2(\nu'; T) \rangle^{1/2} / \langle r^2(\nu; T) \rangle^{1/2}$  for  $T = 100$  K as function of  $\nu'$ . Modes below 0.6 THz in the crystal, or 0.4 THz in the glass contribute about 55%

to the total displacement; 90% are reached only at about 2 THz. This means that the modes which are responsible for the mean square displacement and the Debye-Waller factor are not rigid body motions alone, but contain a significant contribution from intramolecular degrees of freedom.

### 3.5 Debye-Limit and Sound Velocity

Assuming Debye behaviour at very low frequencies  $g(\nu) = 9\nu^2/\nu_D^3$ , we can compare the neutron DOS with the Debye frequency calculated from experimental density and sound velocities:

$$(2\pi\nu_D)^{-3} = \frac{V}{18\pi^2 N} \left( \frac{1}{v_L^3} + \frac{2}{v_T^3} \right) \quad (4)$$

where  $N$  is the number of molecules in volume  $V$ . For the sound velocities of the crystal, we take the average  $\langle v^{-3} \rangle^{-1/3}$  over the three lattice directions of our triple-axis experiment at 200 K. For the glass, we take literature data [57] from Brillouin scattering at 220 K. The so-obtained  $9/\nu_D^3$  are indicated by arrows in Fig. 3.

In both cases, but in particular for the glass, the neutron DOS extrapolates to a far higher Debye level than expected from the sound velocities. Part of the large discrepancy may be due to inaccurate estimates for the sound velocity (see tables) (for instance, the velocities from Brillouin scattering are based on a temperature extrapolation of the refraction index) or due to the circumstance of a broad tail of the resolution of IN6 and a boson peak of OTP which is located at exceptionally low frequency. But for the main part, we must conclude that our neutron scattering experiment on the glass simply does not reach the Debye regime.

In many other glass forming systems, similar discrepancies between DOS and sound velocities are established as well [58, 59, 60], although in some substances a better accord is found [61, 62]. Anyway, our data leave the possibility open that the low-frequency spectrum of the glass and the crystal contain non-harmonic, relaxational contributions, as have been found recently by light scattering [63, 64] or additional glassy excitation.

### 3.6 Heat Capacity

For a harmonic solid, the heat capacity is given by the integral

$$c_p(T) \simeq c_V(T) = N_{\text{at}} R \int_0^\infty d\nu g(\nu) \frac{(\beta/2)^2}{\sinh^2(\beta/2)}. \quad (5)$$

With a Debye DOS, this yields the well-known  $c_p \propto T^3$ . Therefore, in Fig. 5 experimental data [65] for the specific heat of glassy and polycrystalline OTP are plotted as  $c_p/T^3$ . In this representation, a boson peak at 0.35 THz is expected to lead to a maximum at about 4 K.

The lines which are calculated through (5) from the neutron DOS agree for both glass and crystal in absolute

units and over a broad temperature range with the measured data. Similar accord has been reported for a number of other systems [41, 43, 47, 62, 66].

At higher temperatures, the heat capacities of crystalline and glassy OTP differ only little (*e.g.* at 200 K:  $c_p^{\text{cryst}} = 182.8 \text{ J mol}^{-1} \text{ K}^{-1}$  and  $c_p^{\text{glass}} = 186.1 \text{ J mol}^{-1} \text{ K}^{-1}$  [65]). Towards high frequencies, the DOS becomes less sensitive to the presence or absence of crystalline order (as suggested by the representation Fig. 3 for  $\nu \gtrsim 1 \text{ THz}$ ), and remaining differences (clearly visible in Fig. 2) are largely averaged out by the integral (5).

## 4 Thermal effects

Figures 6–8 show the temperature evolution of vibrations in single crystal, polycrystal and glass.

In the single crystal, some phonons become softer on heating, others become stiffer, depending on their direction, as exemplified in Fig. 6. Broadening could not be observed because the linewidth remained always limited by the resolution of the spectrometer.

The temperature dependence of the different phonons is in accord with results from Raman scattering on a polycrystal [41] where substantial positive and negative frequency shifts and broadening were observed already above 70 K, indicating the presence of anharmonicities even at these low temperatures. The opposite trends in the temperature evolution of different modes ensure that the overall anharmonic effects are small, although individual modes are clearly anharmonic.

Through exceptionally large negative Grüneisen parameters the softening of certain phonons may be related to anisotropic thermal expansion. Negative expansion coefficient have indeed been found in crystalline OTP at much lower temperatures ( $T < 30 \text{ K}$ ) [67].

In the frequency distributions of the polycrystal systematic temperature effects are detected as well (Fig. 7a). In Fig. 7b we find a slight increase in the Debye limit ( $\nu \rightarrow 0$ ) of  $g(\nu)/\nu^2$ , which may be explained by regular thermal expansion and softening — the kind of effects which can be accommodated in the harmonic theory of solids by admitting a temperature-dependent, “quasi-harmonic” density of states  $g(\nu; T)$ .

In the glass the temperature effects are weak; only around 2 THz a systematic change in  $g(\nu)$  may be recognised in Fig. 8a. In the low-frequency DOS, shown as  $g(\nu)/\nu^2$  in Fig. 8b, the temperature variation is stronger than in the polycrystalline counterpart. The increase starts at about 160 K, far below the glass transition.

The same anharmonicity of low-lying modes is also responsible for the temperature dependence of the mean square displacement. Fig. 4 shows that  $\langle r^2(T) \rangle$  starts to increase faster than expected from (3) already at about 140 K. These anharmonic contributions to  $\langle r^2(T) \rangle$  amount to about 20% at 200 K for both phases, the crystal being slightly smaller. Note, that around 140 K deviations from the proportionality  $\ln S(Q, \nu = 0) \propto T$  are also observed in coherent elastic scans on the BS instrument IN16. The

additional increase of  $\langle r^2(T) \rangle$  above about 240 K has been consistently interpreted as the onset of fast  $\beta$  relaxation [22]. At higher temperatures, in the presence of quasielastic scattering from relaxational modes, the multi-phonon cross-section becomes ill-defined, and the iterative determination of a DOS is no longer possible.

With a temperature-dependent DOS, the heat capacity can be expressed as [68]

$$c_p(T) = N_{\text{at}} R \int_0^\infty d\nu g(\nu; T) \frac{(\beta/2)^2}{\sinh^2(\beta/2)} \left[ 1 - \left( \frac{\partial \ln \nu}{\partial \ln T} \right)_p \right] \quad (6)$$

where the second term arises explicitly from the shift of phonon modes. The temperature derivative of the logarithmic moment

$$\langle \ln \nu \rangle = \int_0^\infty d\nu g(\nu) \ln \nu \quad (7)$$

can then be taken as a direct measure for the degree of anharmonicity. For Fig. 9, the integral (7) has been evaluated with an upper integration limit  $\nu_g = 5$  THz. From the plot of  $\langle \ln \nu \rangle$  versus  $\ln T$  we estimate slopes  $\partial \langle \ln \nu \rangle / \partial \ln T$  of  $-0.019$  for the polycrystal and  $-0.012$  for the glass. The stronger anharmonicity of the crystal can be traced back to the softening of high-frequency modes.

## 5 Discussion

Our incoherent scattering experiments reconfirm that it is possible to determine a meaningful DOS for a molecular system like OTP. Cross-checks versus  $\langle r^2(T) \rangle$  and  $c_p(T)$  show excellent accord if only the absolute scale of  $g(\nu)$  is corrected for multiple-scattering effects.

By coherent scattering on a single crystal low-lying phonon branches could be resolved. The low-frequency peaks in the DOS of the polycrystal can be assigned to zone-boundary modes. Optic phonons and hybridisation are found at rather low frequencies. The excess of  $g(\nu)$  of the glass over the crystal is restricted to frequencies below about 0.5 THz, the region where the crystal possesses mainly acoustic modes. Towards higher frequency, the DOS is less structured in the glass than in the polycrystal, but the overall spectral distribution is rather similar.

The main result of this communication concerns the strong thermal effects as they were manifested earlier close to the glass transition. With increasing temperature, the glass shows less anharmonicity than the polycrystal. However, this may be partly due to a cancellation of opposite effects. An example is provided by different phonon branches of the single crystal for which positive, negative, and nearly vanishing temperature coefficients are found. In both, crystal and glass the anharmonic contributions to the mean square displacement occur above  $\sim 150$  K. However, the anomalous increase in  $\langle r^2(T) \rangle$  is much stronger in the glass, leading to the known glass transition anomalies.

Finally, concerning our previous analysis of quasielastic scattering in the supercooled liquid OTP we can state: Hybridisation and coupling between inter- and intramolecular modes plays an important role for frequencies higher than 0.6 THz. As a consequence, the quasielastic scattering, which is confined to below 0.25 THz, is clearly dominated by rigid-body motions and the analysis in terms of relaxations in the framework of the mode coupling theory remains reasonable.

## Acknowledgements

We thank A. Doerk (Institut für Physikalische Chemie, Mainz) for help in purifying several samples. Financial support by BMBF under project numbers 03FU4DOR5 and 03PE4TUM9 is gratefully acknowledged.

## Appendix

The determination of a density of states in absolute units is complicated by the inevitable presence of multiple scattering. In the inelastic spectrum of a glass, most multiple-scattering intensity comes from elastic-inelastic scattering histories [69]. This contribution is nearly isotropic, tends to smear out the characteristic  $Q$  dependence of the phonon scattering, and dominates at small angles where the single-scattering signal is expected to vanish as  $Q^2$ .

In our previous analysis of incoherent scattering from glassy OTP we performed a Monte-Carlo simulation for an ideal harmonic system with given  $g(\nu)$  [24]. Here, we simply expand the scattering function  $S(Q, \nu) = A(\nu) + Q^2 B(\nu) + \dots$  which enables us to estimate the multiple scattering  $A(\nu)$  by  $Q^2 \rightarrow 0$  extrapolation from the  $S(2\theta(Q, \nu), \nu)$  spectra. Results are shown in Fig. 10a. For 200 K, good accord with the Monte-Carlo simulation is found, and measured spectra can be corrected by simply subtracting  $A(\nu)$ . The interplay between multi-phonon scattering and multiple scattering limits this procedure to frequencies  $\nu \lesssim 3$  THz.

In the low-frequency region, the subtraction of  $A(\nu)$  leads to almost the same DOS as the *ad hoc* normalisation of Sect. 3.2. This confirms our assignment of the 16 modes below the gap, and it shows at the same time that multiple scattering is indeed the main obstacle to a quantitative determination of a generalised density of vibrational states.

## References

1. J. N. Andrews and A. R. Ubbelohde, Proc. Roy. Soc. A **228**, 435 (1955).
2. E. McLaughlin and A. R. Ubbelohde, Trans. Faraday Soc. **54**, 1804 (1958).
3. R. J. Greet and D. Turnbull, J. Chem. Phys. **46**, 1243 (1967).
4. W. T. Laughlin and D. R. Uhlmann, J. Chem. Phys. **76**, 2317 (1972).

5. M. Cukierman, J. W. Lane and D. R. Uhlmann, *J. Chem. Phys.* **59**, 3639 (1973).
6. K. U. Schug, H. E. King and R. Böhmer, *J. Chem. Phys.* **109**, 1472 (1998).
7. G. Williams and P. J. Hains, *Chem. Phys. Lett.* **10**, 585 (1971).
8. G. Williams and P. J. Hains, *Faraday Symp. Chem. Soc.* (1972).
9. G. D'Arrigo, *J. Chem. Phys.* **63**, 61 (1975).
10. A. Vasquez and P. A. Flinn, *J. Chem. Phys.* **72**, 1958 (1980).
11. G. Fytas, C. H. Wang, D. Lilge and T. Dorfmueller, *J. Chem. Phys.* **75**, 4247 (1981).
12. P. K. Dixon and S. R. Nagel, *Phys. Rev. Lett.* **61**, 341 (1988).
13. G. Meier and E. W. Fischer, *Springer Proceedings in Physics* **29**, 122 (1988).
14. E. W. Fischer, C. Becker, J. U. Hagenah and G. Meier, *Progr. Coll. Polym. Sci.* **80**, 198 (1989).
15. G. P. Johari and M. Goldstein, *J. Phys. C* **74**, 2034 (1970).
16. G. P. Johari and M. Goldstein, *J. Chem. Phys.* **53**, 2372 (1970).
17. L. Wu and S. R. Nagel, *Phys. Rev. B* **46**, 11198 (1992).
18. W. Götze, in *Liquids, Freezing and the Glass Transition*, edited by J. P. Hansen, D. Levesque and D. Zinn-Justin (Les Houches, session LI), North Holland: Amsterdam (1991).
19. W. Götze and L. Sjögren, *Transp. Theory Stat. Phys.* **24**, 801 (1995).
20. H. Z. Cummins, *J. Phys. Condens. Matter* **11**, A95 (1999).
21. E. Bartsch *et al.*, *Ber. Bunsenges. Phys. Chem.* **93**, 1252 (1989).
22. W. Petry *et al.*, *Z. Phys. B* **83**, 175 (1991).
23. M. Kiebel *et al.*, *Phys. Rev. B* **45**, 10301 (1992).
24. J. Wuttke *et al.*, *Z. Phys. B* **91**, 357 (1993).
25. A. Tölle *et al.*, *Phys. Rev. Lett.* **80**, 2374 (1998).
26. E. Bartsch *et al.*, *Phys. Rev. E* **52**, 738 (1995).
27. A. Tölle, H. Schober, J. Wuttke and F. Fujara, *Phys. Rev. E* **56**, 809 (1997).
28. A. Tölle *et al.*, *Eur. Phys. J. B* **5**, 231 (1998).
29. W. Steffen *et al.*, *Phys. Rev. E* **49**, 2992 (1994).
30. A. P. Sokolov, W. Steffen and E. Rössler, *Phys. Rev. E* **52**, 5015 (1995).
31. H. Z. Cummins *et al.*, *Prog. Theor. Phys. Suppl.* **126**, 21 (1997).
32. U. Bengtzelius, W. Götze and A. Sjölander, *J. Phys. C* **17**, 5915 (1984).
33. J. Bosse and J. S. Thakur, *Phys. Rev. Lett.* **59**, 998 (1987).
34. T. Franosch *et al.*, *Phys. Rev. E* **56**, 5659 (1997).
35. R. Schilling and T. Scheidsteiger, *Phys. Rev. E* **56**, 2932 (1997).
36. T. Franosch *et al.*, *Phys. Rev. E* **55**, 7153 (1997).
37. M. Fuchs, W. Götze and M. R. Mayr, *Phys. Rev. E* **58**, 3384 (1998).
38. A. J. Leadbetter, *J. Chem. Phys.* **51**, 779 (1969).
39. F. Gompf, J. S. Lannin, *J. Phys. (Paris), Colloque* **42**, 27 (1981).
40. F. Gompf, *J. Phys. Chem. Solids* **42**, 539 (1981).
41. A. Criado, F. J. Bermejo, A. de Andres and J. L. Martínez, *Mol. Phys.* **82**, 787 (1994).
42. F. J. Bermejo, A. Criado and J. L. Martínez, *Phys. Lett. A* **195**, 236 (1994).
43. F. J. Bermejo *et al.*, *Phys. Rev. B* **53**, 5259 (1996).
44. A. Meyer *et al.*, *Phys. Rev. B* **53**, 12107 (1996).
45. M. T. Dove *et al.*, *Phys. Rev. Lett.* **78**, 1070 (1997).
46. G. J. Cuello *et al.*, *Phys. Rev. B* **57**, 8254 (1998).
47. C. Talón *et al.*, *Phys. Rev. B* **58**, 745 (1998).
48. F. J. Bermejo *et al.*, *Phys. Rev. Lett.* **81** 3801 (1998).
49. G. M. Brown and H. A. Levy, *Acta Cryst. B* **35**, 785 (1979).
50. S. Aikawa, Y. Maruyama, Y. Ohashi and Y. Sasada, *Acta Cryst. B* **34**, 2901 (1978).
51. I. Baraldi and G. Ponterini, *J. Mol. Struct.* **122**, 287 (1985).
52. J. M. Carpenter and C. A. Pelizzari, *Phys. Rev. B* **12**, 2391 (1975).
53. W. R. Busing, *J. Am. Chem. Soc.* **104**, 4829 (1982).
54. D. Kirin, V. Volovšek and R. M. Pick, *J. Mol. Struct.* **482-483**, 421 (1999).
55. U. Buchenau, A. Wischnewski, D. Richter and B. Frick, *Phys. Rev. Lett.* **77**, 4035 (1996).
56. For a meaningful application of (3), we have to assume the rigid-body limit (Sect. 3.1, Ref. [24]). Therefore,  $M$  has to be taken as the average atomic mass which in the case of OTP is 7.2.
57. Y. Higashigaki and C. H. Wang, *J. Chem. Phys.* **74**, 3175 (1981).
58. U. Buchenau *et al.*, *Europhys. Lett.* **6**, 695 (1988).
59. L. Gil, M. A. Ramos, A. Bringer and U. Buchenau, *Phys. Rev. Lett.* **70**, 182 (1993).
60. A. Wischnewski *et al.*, *Phil. Mag. B* **77**, 579 (1998).
61. R. Zorn *et al.*, *Phys. Rev. E* **52**, 781 (1995).
62. J. Wuttke, W. Petry, G. Coddens and F. Fujara, *Phys. Rev. E* **52**, 4026 (1995).
63. G. Monaco *et al.*, *Phys. Rev. Lett.* **82**, 1776 (1999).
64. G. Monaco *et al.*, preprint
65. S. S. Chang and A. B. Bestul, *J. Chem. Phys.* **56**, 503 (1972).
66. U. Buchenau *et al.*, *Phys. Rev. B* **34**, 5665 (1986).
67. M. A. Ramos, S. Vieira, F. J. Bermejo and J. L. Martínez, *Mol. Phys.* **85**, 1037 (1995).
68. J. C. K. Hui and P. B. Allen, *J. Phys. C* **8**, 2923 (1975).
69. V. Sears, *Adv. Phys.* **24**, 2 (1975).
70. G. Monaco, L. Comez and D. Fioretto, *Philos. Mag. B* **77**, 463 (1998).
71. G. Monaco, C. Masciovecchio, G. Ruocco and F. Sette, *Phys. Rev. Lett.* **80**, 2161 (1998).

**Figure captions:**

Figure 1:

Phonon dispersion relations of crystalline orthoterphenyl as measured on the triple axis spectrometer IN12 at 200 K. The wave vectors are given in reciprocal lattice units.

Figure 2:

Renormalized density of vibrational states of glassy ( $\square$ ) and crystalline OTP ( $\blacksquare$ ) at 100 K obtained from IN6.

Figure 3:

Density of vibrational states of glassy ( $\square$ ) and crystalline OTP ( $\blacksquare$ ) at 200 K. To emphasise the excess density of states of the glass over the crystal  $g(\nu)/\nu^2$  is shown. The arrows mark the Debye limit  $\nu \rightarrow 0$  calculated from sound velocities and densities (at 220 K for the glass and at 200 K for the crystal).

Figure 4:

Mean square displacement  $\langle r^2(T) \rangle$  of glassy OTP from elastic back-scattering (IN13,  $\diamond$ ) and from time-of-flight spectra (IN6, plateau value of  $S(q, t)$ ,  $\square$ ). For comparison, IN6 data of polycrystalline OTP are also shown ( $\blacksquare$ ). The lines are calculated from the densities of states at 100 K of the glass (dashed) and the polycrystal (solid line). The inset shows the relative value of  $d = \langle r^2 \rangle^{1/2}$  at 100 K for the crystal and the glass when the integral (3) is restricted to modes with  $0 < \nu < \nu'$ .

Figure 5:

Experimental heat capacity capacities  $c_p/T^3$  of glassy and crystalline OTP [65], compared to  $c_p/T^3$  calculated from the density of vibrational states  $g(\nu)$  at 100 K.

Figure 6:

Examples for the temperature dependence of phonons along different directions. Hardening (left, note the negative energy scale), softening (middle) Our data leave the possibility open that the low-frequency spectrum of the glass and the crystal contains non-harmonic, relaxational contributions. and nearly no temperature variation (right) is observed with increasing temperature. The intensities are Bose corrected. The remaining differences are due to the use of different set-ups (collimation).

Figure 7:

(a) Vibrational density of states of polycrystalline OTP for three different temperatures. Note the significant temperature dependence of the DOS for all frequencies. — (b) To emphasise the temperature evolution at small energies, the same data are plotted as  $g(\nu)/\nu^2$ . The temperature dependence of the low-frequency modes becomes apparent.

Figure 8:

(a) Temperature dependence of the vibrational density of states of glassy OTP. — (b) The low frequency region of (a) plotted as  $g(\nu)/\nu^2$ . Above 160 K the density of low-frequency modes increases strongly.

Figure 9:

The logarithmic moment  $\langle \ln \nu \rangle$  versus  $\ln T$  of the density of states of glassy and crystalline OTP. From the straight line, one obtains the slope  $\partial \langle \ln \nu \rangle / \partial \ln T$  which is a measure for the anharmonicity.

Figure 10:

(a) Comparison of the experimental data at two scattering angles with the multiple scattering contribution obtained

by an  $Q^2 \rightarrow 0$  extrapolation. The MS nearly completely dominates the scattering signal at small angles. — (b) Comparison of the density of states obtained from the MS-corrected spectra with the *ad hoc* normalized DOS.

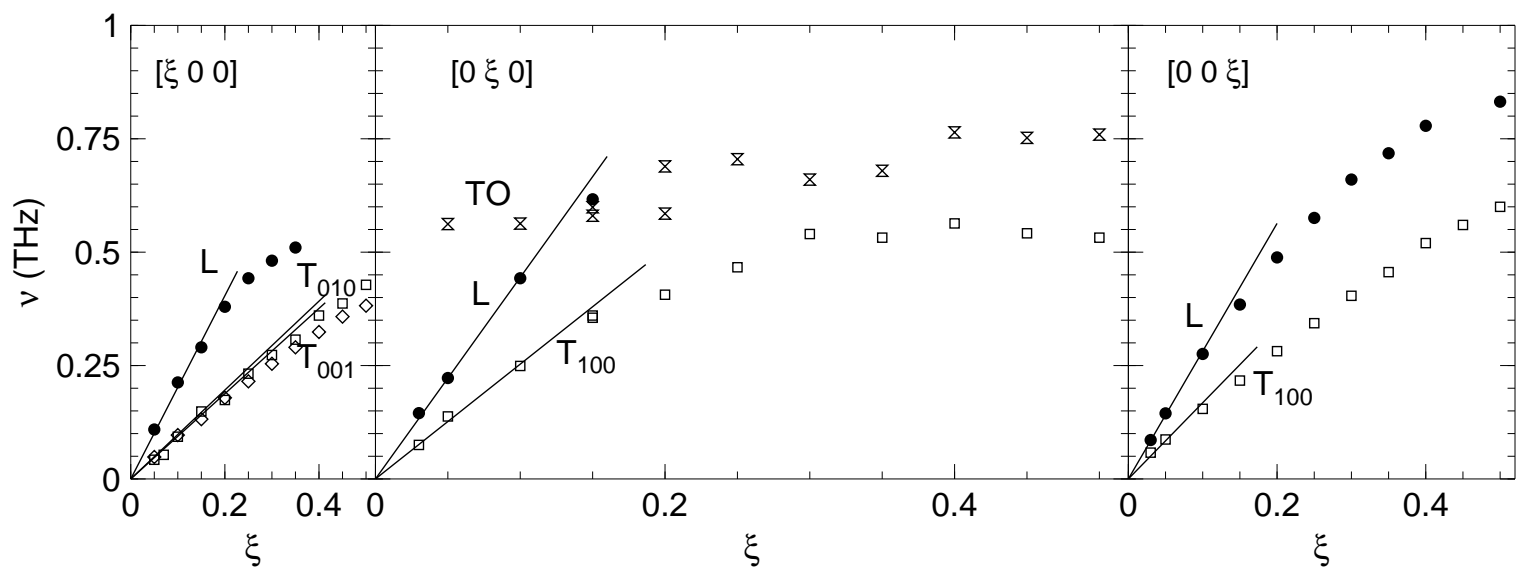
**Table 1.** Sound velocities (in km/s) for three phonon branches and different lattice directions, obtained from linear fits to the low- $q$  limit of the measured phonon dispersions.

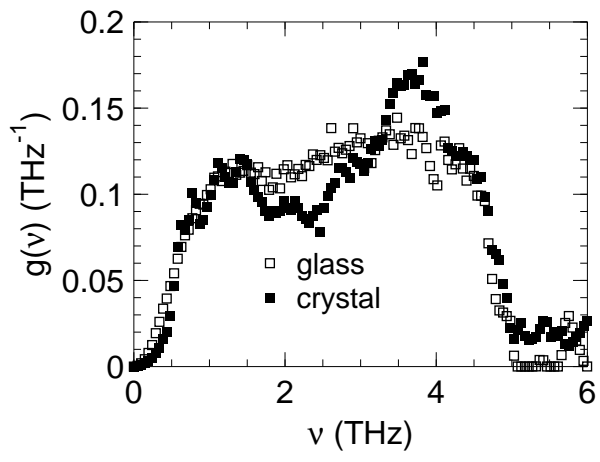
	$v_{[100]}$	$v_{[010]}$	$v_{[001]}$	$\langle v \rangle$	$\langle v^{-3} \rangle^{-1/3}$
$v_L$	3.71	2.68	3.30	3.23	3.11
$v_{T_1}$	1.82	1.52	1.97	1.75	1.71
$v_{T_2}$	1.67	–	–		

**Table 2.** Sound velocities in the glass as measured by Brillouin scattering, using visible light or X-rays.

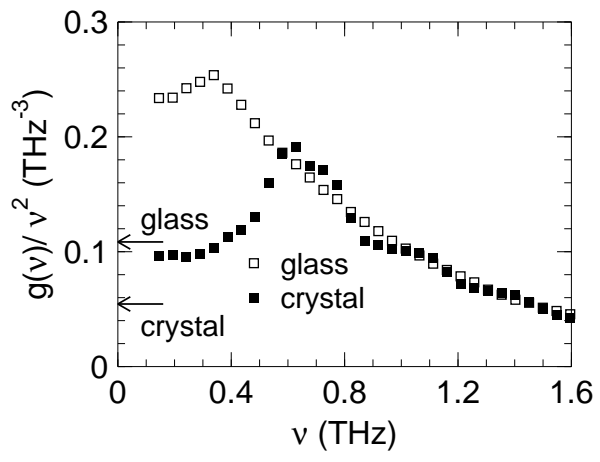
$T$ (K)	$v_L$ (km/s)	$v_T$ (km/s)	method	reference
220	2.94	1.37	light	[57]
223	2.63		light	[70]
200	2.70		X-rays	[71]

Tölle et al. Figure 1

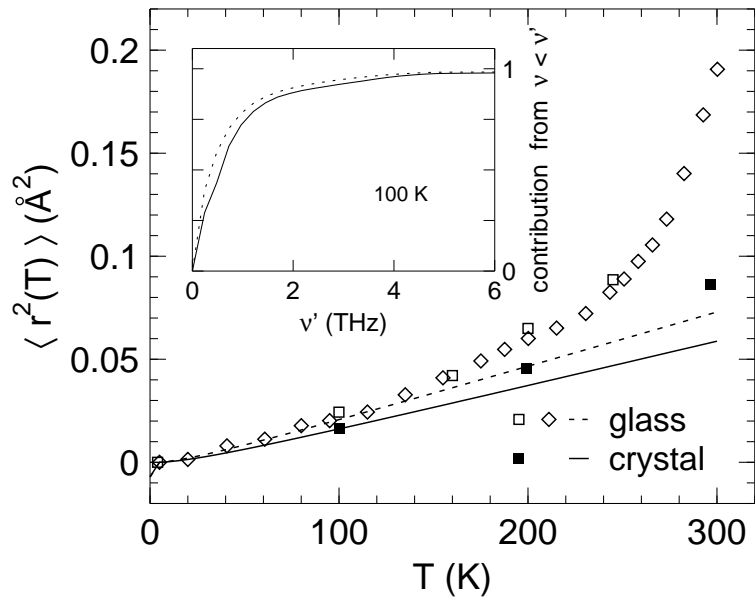




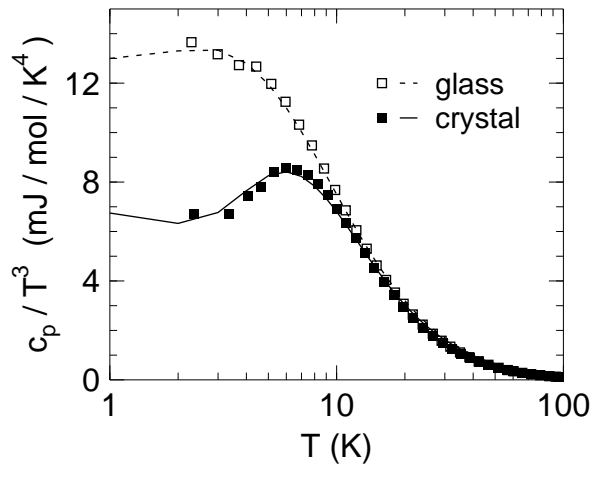
Tölle et al. Figure 2



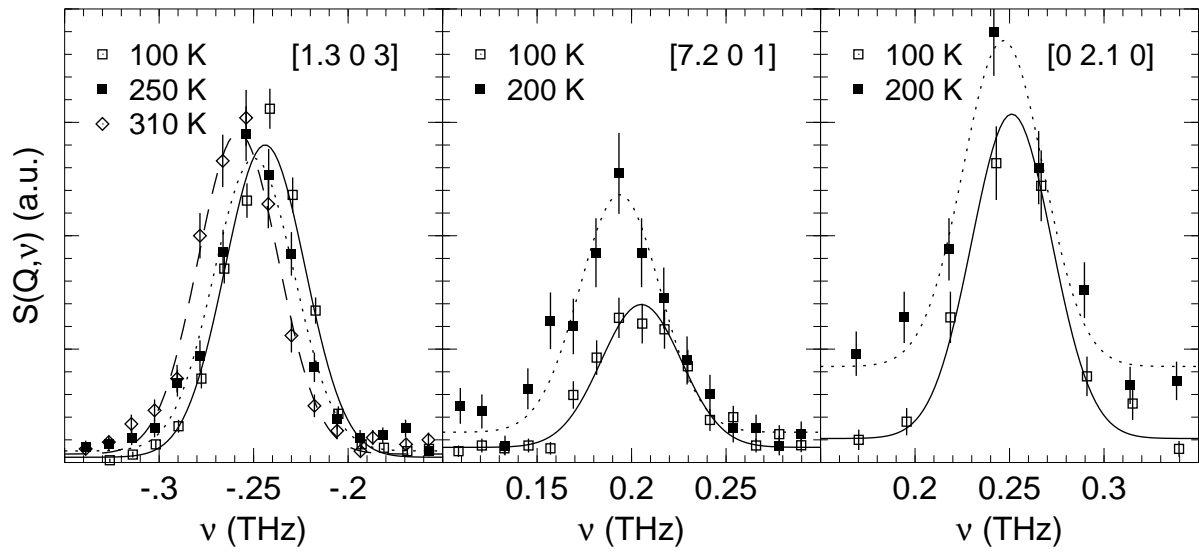
Tölle et al. Figure 3



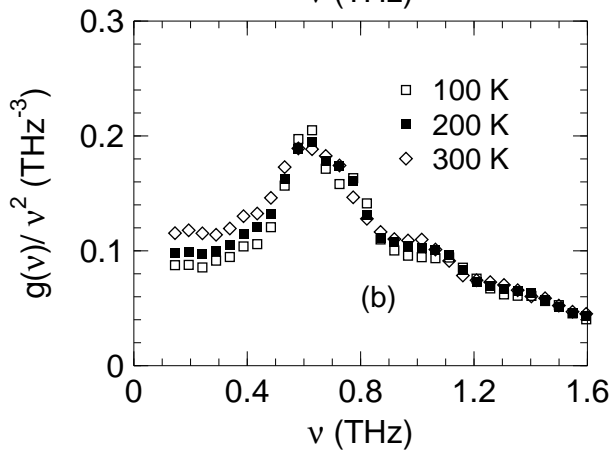
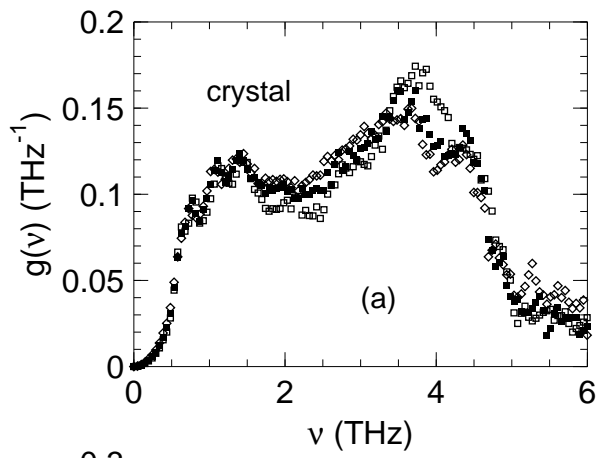
Tölle et al. Figure 4



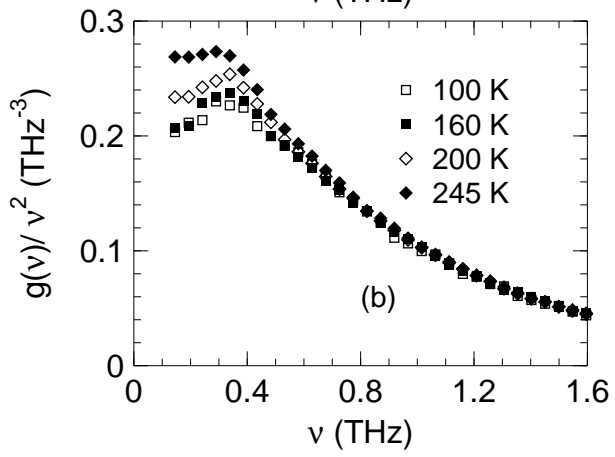
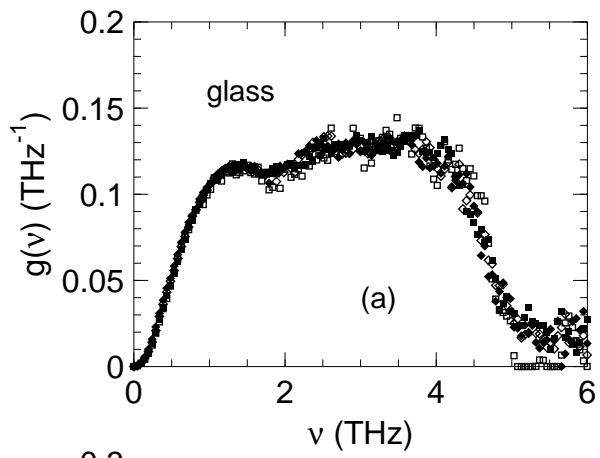
Tölle et al. Figure 5



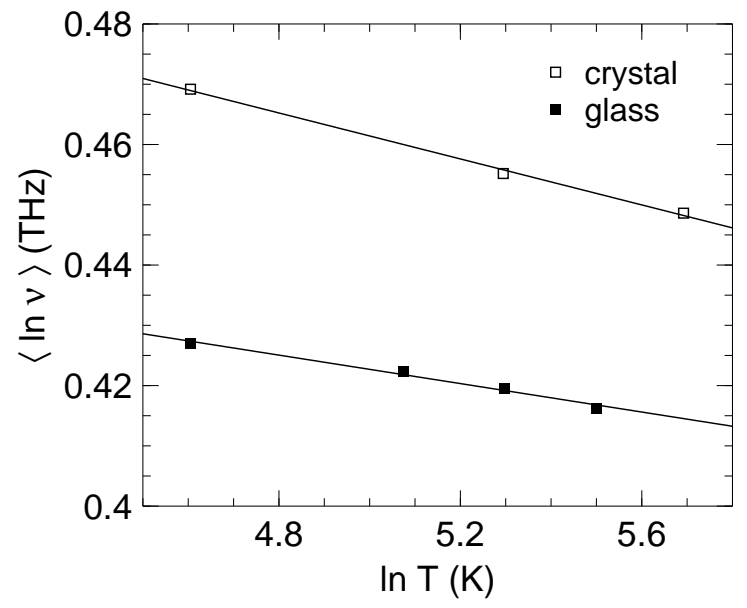
Tölle et al. Figure 6



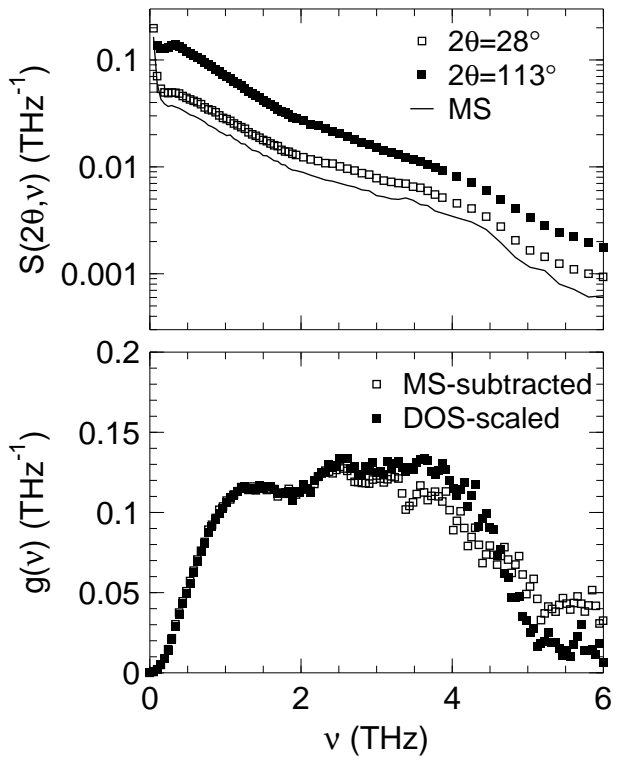
Tölle et al. Figure 7a,b



Tölle et al. Figure 8a,b



Tölle et al. Figure 9



Tölle et al. Figure 10a,b